Remote Sens. **2010**, *2*, 2509-2530; doi:10.3390/rs2112509

OPEN ACCESS

Remote Sensing

ISSN 2072-4292

www.mdpi.com/journal/remotesensing

Article

Seven Years' Observation of Mid-Upper Tropospheric Methane from Atmospheric Infrared Sounder

Xiaozhen Xiong [1,2,*], Chris Barnet [2], Eric Maddy [1,2], Jennifer Wei [1,2], Xingpin Liu [1,2] and Thomas S. Pagano [3]

[1] Dell Perot Systems Government Services, Fairfax, VA 22031, USA

[2] Center for Satellite Applications and Research (STAR), National Environmental Satellite, Data, and Information Service (NESDIS), NOAA, Camp Springs, MD 20746, USA; E-Mails: Chris.barnet@noaa.gov (C.B.); Eric.maddy@noaa.gov (E.M.); Jennifer.wei@noaa.gov (J.W.); Xingpin.liu@noaa.gov (X.L.)

[3] NASA/Jet Propulsion Laboratory, Pasadena, CA, USA; E-Mail: Thomas.s.pagano@jpl.nasa.gov

* Author to whom correspondence should be addressed; E-Mail: Xiaozhen.xiong@noaa.gov; Tel.: +1-301-316-5020; Fax: +1-301-238-2398.

Received: 20 September 2010; in revised form: 28 October 2010 / Accepted: 5 November 2010 / Published: 9 November 2010

Abstract: The Atmospheric Infrared Sounder (AIRS) on EOS/Aqua platform provides a measurement of global methane (CH_4) in the mid-upper troposphere since September, 2002. As a thermal infrared sounder, the most sensitivity of AIRS to atmospheric CH_4 is in the mid-upper troposphere with the degree of freedom of ~1.0. Validation of AIRS CH_4 product *versus* thousands of aircraft profiles (convolved using the AIRS averaging kernels) demonstrates that its RMS error (RMSE) is mostly less than 1.5%, and its quality is pretty stable from 2003 to 2009. For scientific analysis of the spatial and temporal variation of mid-upper tropospheric CH_4 (MUT-CH_4) in the High Northern Hemisphere (HNH), it is more valuable to use the AIRS retrieved CH_4 in a layer of about 100 hPa below tropopause ("Representative Layer") than in a fixed pressure layer. Further analysis of deseasonalized time-series of AIRS CH_4 in both a fixed pressure layer and the "Representative Layer" of AIRS (only for the HNH) from 2003 to 2009 indicates that, similar to the CH_4 in the marine boundary layer (MBL) that was found to increase in 2007–2008, MUT-CH_4 was also observed to have a recent increase but the most significant increase occurred in 2008. MUT-CH_4 continued to increase in 2009, especially in the HNH. Moreover, the trend of MUT-CH_4 from 2006 to 2008 is lower than the trend of CH_4 in the MBL by 30–40% in both the southern hemisphere and HNH. This delay for the MUT-CH_4 increase of about

one year than CH_4 in the MBL as well as the smaller increase trend for MUT-CH_4 suggest that surface emission is likely a major driver for the recent CH_4 increase. It is also found that the seasonal cycle of MUT-CH_4 is different from CH_4 in the MBL due to the impact of transport, in addition to the surface emission and the photochemical loss.

Keywords: methane; mid-upper troposphere; satellite; AIRS; trend; seasonal cycle

1. Introduction

As one of the most important greenhouse gases, atmospheric methane (CH_4) is 25 times more effective on a per unit mass basis than carbon dioxide in absorbing long-wave radiation on a 100-year time horizon, and accounts for 18% of the total of 2.66 W m^{-2} of the anthropogenically produced greenhouse gas radiative forcing [1]. The concentration of CH_4 over the globe has risen dramatically since the preindustrial era [2-4]. However, CH_4 mixing ratio is almost stable since 2000 [5,6], and a renewed increase was found in 2007 and 2008 [7,8]. The increase of CH_4 in 2007 was believed to be largely caused by wetlands with a large tropical contribution [7], and Dlugokencky *et al.* [8] suggested the most likely drivers of the CH_4 anomalies during 2007 and 2008 were greater than average precipitation in the tropics plus anomalously high temperatures in the Arctic, however it is still hard to quantify the impacts from different sources in different regions. One large uncertainty in the quantification of methane emissions can be from the high northern latitude regions [9]. For example, CH_4 is found to release from both thawing lakes and soils [10], and Shakhova *et al.* [11] recently reported convincing evidence of CH_4 outgassing from the Arctic continental shelf off northeastern Siberia (Laptev and East Siberia Sea).

In recent years, space-borne remote sensing has been employed for the measurement of CH_4 with large spatial and temporal coverage. Two major types of measurement are the measurement of the total column using the near-infrared (NIR) spectrum and the measurement of the MUT-CH_4 using the thermal infrared (TIR) spectrum. The NIR measurements in operation include the SCanning Imaging Absorption spectroMeter for Atmospheric CHartographY (SCIAMACHY) instrument onboard ENVISAT [12], and the Greenhouse gases Observation SATellite (GOSAT) which carries the Thermal And Near-infrared Sensor for carbon Observation (TANSO) [13]. The TIR measurements in operation include the Tropospheric Emission Spectrometer (TES) on NASA Earth Observing System (EOS) Aura mission [14], the AIRS on EOS Aqua mission [15], and the Infrared Atmospheric Sounding Interferometer (IASI) on European polar Meteorological Operational Platform (METOP-1) [16,17]. GOSAT also carries TIR measurement.

As one of the space-borne thermal infrared sounders in operation, AIRS was launched in polar orbit (13:30, ascending node) on the EOS/Aqua satellite in May 2002. It is the first hyperspectral infrared sounder designed to support weather forecast [15] and CH_4 is one of the research products. AIRS has been very stable since its launch in 2002 [18], and has provided more than eight years' observation of CH_4. This paper reviews the characteristics of the data from this sensor (Section 2) and its validation (Section 3). Since only about one piece of information of CH_4 can be obtained (the degree of freedom is ~1.0) from AIRS, it is important to determine which layer from the AIRS retrieved CH_4 profile can

be best used to analyze the variation of MUT-CH_4 with the least artificial impact from the sensor itself and the retrieval algorithm. The use of the AIRS retrieved CH_4 in a layer about 100 hPa below tropopause and its comparison with *in situ* aircraft measurements is also discussed in Section 3. Section 4 analyzes the deseasonalized time-series of MUT-CH_4 in a fixed pressure layer and the "representative layer" (for the HNH only), as well as its comparison with the CH_4 in the lower troposphere from ground-based measurements. A summary and conclusions are given in Section 5.

2. Characteristics of CH_4 Retrieval from AIRS

AIRS has 2,378 channels covering 649–1,136, 1,217–1,613 and 2,169–2,674 cm^{-1} at high spectral resolution ($\lambda/\Delta\lambda = 1200$), and the noise, which is represented as the equivalent change in temperature (NeΔT) at a reference temperature of 250 K, ranges from 0.14 K in the 4.2 μm lower tropospheric sounding wavelengths to 0.35 K in the 15 μm upper tropospheric sounding region [15]. The spatial resolution of AIRS is 13.5 km at nadir, and in a 24-hour period AIRS nominally observes the complete globe twice per day. For retrieval in both clear and partial cloudy scenes, 9 AIRS fields-of-view within the footprint of the Advanced Microwave Sounding Unit (AMSU) are used to derive a single cloud-cleared radiance spectrum in a field-of-regard (FOR). The cloud-cleared FOR radiance spectrum is then used for retrieving profiles with a spatial resolution of about 45 km. The CH_4 first guess profile, which is also the "*a priori*" mean profile, in the retrieval is given as a function of latitude and pressure (to capture its strong latitudinal and vertical gradients), and is generated by using a non-linear polynomial fitting to some *in situ* aircraft measurements and model data [19]. The atmospheric temperature profile, water profile, surface temperature and surface emissivity required as inputs in CH_4 retrieval are derived from other AIRS channels using the version 5 of AIRS product retrieval software. These data are available at the NASA Goddard Earth Sciences Data and Information Services Center (DISC) (http://disc.gsfc.nasa.gov/AIRS/index.shtml/). An "off-line" version of the AIRS product is run at NOAA National Environmental Satellite, Data, and Information Service (NESDIS), Center for Satellite Application and Research (STAR), where the data are thinned to a 3° × 3° spatial grid, and these data are available at NOAA/NESDIS/STAR by request. The data from NOAA are routinely reprocessed with algorithm updates.

2.1. Sensitivities of AIRS

71 CH_4 channels near 7.6 μm H_2O band are used in the retrieval. To illustrate the sensitivities of AIRS, we first define it as the change in brightness temperature divided by the thickness of layer ($\Delta T/\Delta Z$, unit: K/km). Figure 1 shows the sensitivities of these AIRS channels for a 2% change of CH_4 mixing ratio in different layers for three typical profiles in polar, tropics and mid-latitude region respectively. It is evident that the most sensitive layers are in the mid-upper troposphere. Given that the methane band resides inside the broad 7.6 μm H_2O band, the moisture optical depth pushes the CH_4 peak sensitivity upwards, so for the peak CH_4 absorption channels (red lines), the most sensitive layers are at 150–300 hPa in the tropics, and 200–400 hPa in the mid-latitude region. The most sensitive layers for weak CH_4 absorption channels (dark lines) are at an altitude of about 50–100 hPa lower than those of the peak channels in the tropics and mid-latitude regions. In the polar, the most sensitive layers are at 300–600 hPa, and the sensitivities are much less than in the tropics and mid-latitude

regions. Obviously, from Figure 1 we can see the information from these channels is redundant, so seven retrieval layers are used, which are 0.016–36 hPa, 36–160 hPa, 160– 260 hPa, 260–359 hPa, 359–460 hPa, 460–596 hPa, and 596–1,100 hPa (marked with dark dash lines in the top panel of Figure 1). The thickness of layer is about 100 hPa in the most sensitive regions between 150 and 600 hPa. For a more accurate computation of the radiative transfer in the atmosphere, the atmosphere is divided into 100 layers [20].

Figure 1. AIRS sensitivity (ΔT/ΔZ, unit: K/km) for a 2% change in CH_4 mixing ratio for atmosphere profiles in polar, tropics and mid-latitude respectively. Each line represents the sensitivity for each of the 71 AIRS channels used in the retrieval. The locations of these 71 channels in the AIRS spectrum are marked as colored squares in the bottom panel, and the red squares represent peak absorption channels near 13,06 cm^{-1}, and the black squares represent far wing weak absorption channels. The bottom panel is the change of brightness temperature (ΔT, unit: K) in the spectrum spanning from 1,210 to 1,400 cm^{-1} for a 2% change in the total column of CH_4 for polar, tropics and mid-latitude profiles respectively. Blue crosses are the noise level of AIRS channels.

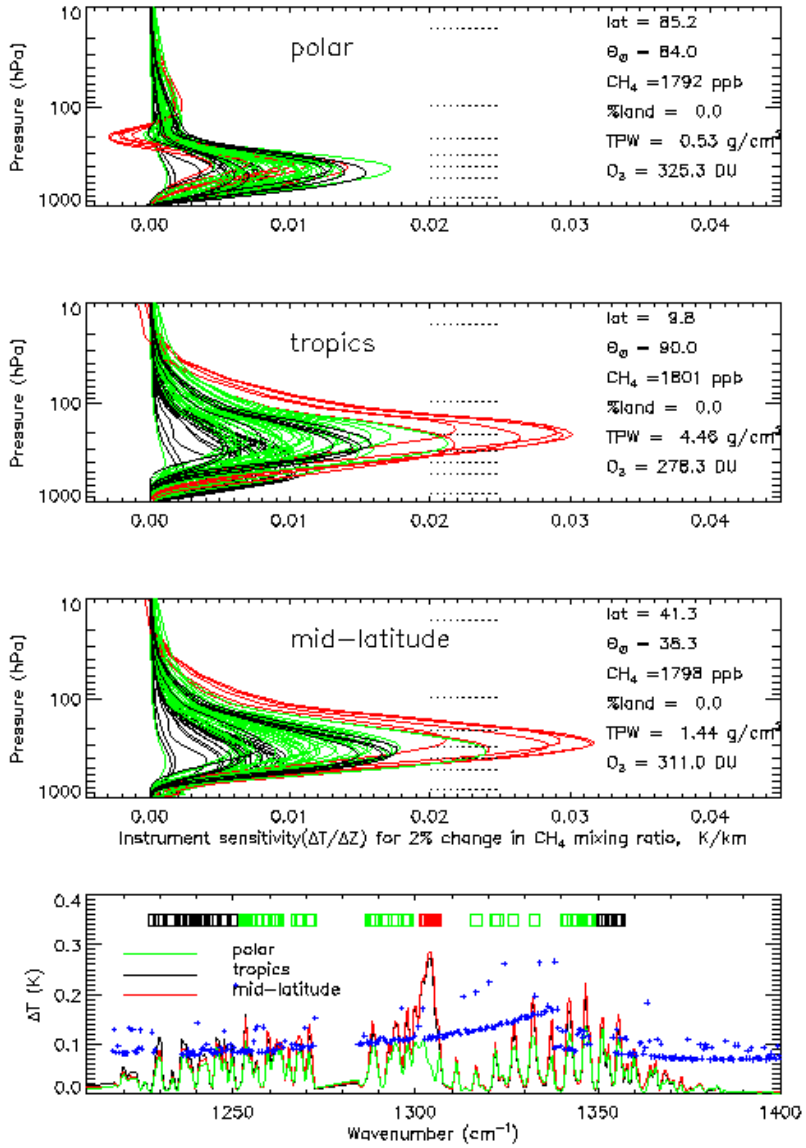

In the bottom panel of Figure 1, we can see that for a 2% change of CH_4 total column in the atmosphere, the changes of brightness temperature (ΔT) in CH_4 spectrum for the tropical profile and mid-latitude profile are very similar, and they are significantly larger than the noise level in the channels near 1,306 cm^{-1}. However, for the polar profile the ΔT for most channels are close to the noise level. These indicate that in the tropics and the mid-latitude regions, AIRS can detect a 2% change or less of the total column of CH_4; however in the polar region, AIRS can barely detect a 2% change.

2.2. Variation of Degree of Freedom (DOF)

In the AIRS retrieval algorithm, the retrieval solution is obtained by finding the eigenvectors and eigenvalues of the covariance matrix of the sensitivity, weighted by an inverse of the estimates of the precision and accuracy of our radiative transfer model and the errors and noise in the measurements. The corresponding eigenvalues give an indication of the usefulness of each component and the component corresponding to small eigenvalues is thrown away or heavily damped in order to get a stable solution. We define the degrees of freedom (DOF) as the fractional number of significant eigenfunctions used in the retrieval process, so variation of DOFs reflects the change of sensitivity of the retrieval, and represents how much portion of the retrieved value is from the satellite observation approximately (the rest is from the "*a priori*"). As an example, Figure 2 shows the variation of DOFs in two regions, and on average the DOFs over South Asia and Alaska-Canada are 1.03 ± 0.11(10.6%) and 0.67 ± 0.068 (10.2%), respectively. Overall, DOFs in the lower latitude regions are larger than in the high latitude regions, in summer is larger than in winter, and during the daytime is larger than during the nighttime. Due to the impact of Asian summer monsoon, which brings more moisture into South Asia and induces deep convection, variation of DOFs in South Asia is pronounced. Over Alaska-Canada the DOFs are anti-correlated with the tropopause height represented in hPa and the correlation coefficient is −0.70, and that means the higher the tropopause height (corresponding to a smaller pressure level), the larger the DOF. Lower DOFs in the polar region in winter are mainly due to the lower lapse rate. In general, the relationship between tropopause height and DOF is not obvious if compared to the fact that the lower lapse rate leads to lower DOF. As the DOFs in winter are smaller than in summer, measurement of CH_4 from space is more difficult in winter season in the polar region. Considering the large variation of tropopause in the HNH, using the retrieved CH_4 in a layer 50 to 250 hPa below tropopause to analyze CH_4 variation in the real atmosphere is better than using CH_4 in a fixed pressure layer [21].

Due to the temporal and spatial variation of DOFs, some of the variation in the retrieved CH_4 is from artificial effects, which adds more complexity in analyzing CH_4 variation in the real atmosphere using the retrieved CH_4 data alone. For example, in cases when the DOF are small, the retrieved values are mostly from the "*a priori*". A rough estimate indicates that the uncertainty attributed to the variation of DOF is less than 0.8% in the high northern hemisphere [22] and 0.3% over South Asia. This artificial impact has to be taken into account when analyzing the satellite retrieval product derived from any thermal infrared sounder, and while comparing the retrieval products with model simulations and/or *in situ* measurements, it is strongly recommended to apply the averaging kernels [19,23]. The trace of the averaging kernel matrix is equivalent to DOF.

Figure 2. Seasonal variation of Degree of Freedom (DOF) in two regions: South Asia (80–110°E, 20–35°N) and Alaska-Canada (165–90°W, 60–70°N). Lower panel shows the anti-correlation between DOFs and the tropopause height over Alaska-Canada.

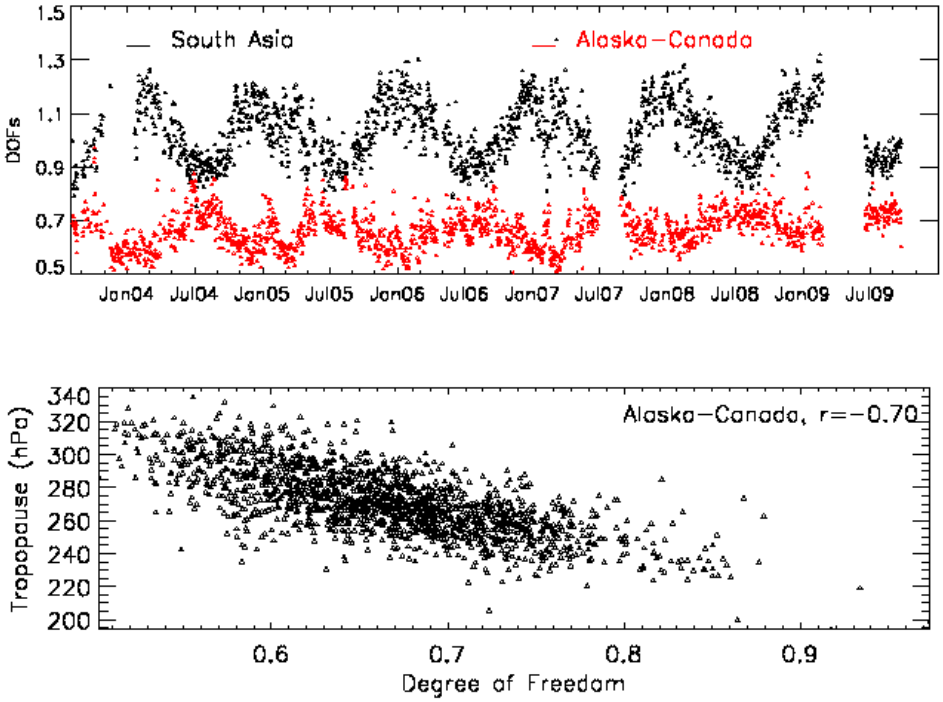

3. Validation of AIRS CH_4

3.1. Validation Data Set

In situ aircraft measurements of CH_4 profiles are used for validations, which include (1) the profiles from NOAA Earth System Research Laboratory, Global Monitoring Division (NOAA/ESRL/GMD) Carbon Cycle Group obtained by routinely collecting air samples on biweekly to monthly aircraft flights at over twenty sites; (2) the profiles from specific campaigns, such as the Intercontinental Chemical Transport Experiment (INTEX) A and –B, Stratosphere-Troposphere Analyses of Regional Transport in 2008 (START08) and The Arctic Research of the Composition of the Troposphere from Aircraft and Satellites (ARCTAS).

(1) NOAA/ESRL/GMD aircraft measurements: Air samples are collected using turboprop aircraft with maximum altitude limits of 300–350 hPa. Individual flights required about 1.5 hours to complete. Measurements are made by collecting samples of air (approximately 0.7 liter volume at 40 psa) in glass containers. Twelve to twenty flasks are held in a suitcase-sized container, and collection of air in a single flask at a unique altitude allows a sampling vertical resolution of up to 400 m in the boundary layer. After each flight the flask packages are shipped to the NOAA laboratory in Boulder, Colorado for trace gas analysis. Table 1 lists the locations of these sites and their profile number used in validation.

(2) The INTEX-A field mission was conducted in the summer of 2004 (1 July to 15 August 2004) over North America (NA) and the Atlantic. This effort had a broad scope to investigate the

transport and chemistry of long-lived greenhouse gases, oxidants and their precursors, aerosols and their precursors, as well their relationship with radiation and climate. NASA's DC-8 and J-31 were joined by aircraft from a large number of European and North American partners to explore the composition of the troposphere over NA and the Atlantic as well as radiative properties and effects of clouds and aerosols in a coordinated manner [24]. An air sample is collected in a conditioned, evacuated 2-L stainless steel canister equipped with a bellows valve, and is returned to the UC-Irvine laboratory for CH4 analysis using gas chromatography (GC, HP-5890A) with flame ionization detection. The use of the primary CH4 calibration standards dating back to late 1977 ensures that these measurements are internally consistent. The measurement accuracy is ±1% and the analytical precision at atmospheric mixing ratios is about 1 ppbv [6, 25].

(3) INTEX-B was a major NASA led multi-partner atmospheric field campaign completed in the spring of 2006 (http://cloud1.arc.nasa.gov/intex-b/). INTEX-B was performed in two phases. In its first phase (1–21 March), INTEX-B operated as part of the MILAGRO campaign with a focus on observations over Mexico and the Gulf of Mexico. In the second phase (17 April–15 May), the main INTEX-B focus was on trans-Pacific Asian pollution transport. Multiple airborne platforms carrying state of the art chemistry and radiation payloads were flown in concert with satellites and ground stations during the two phases of INTEX-B [26]. The CH4 aircraft measurements in INTEX-B are similar to INTEX-A.

(4) START08 was conducted using the NSF/NCAR Gulfstream V research aircraft during April–June 2008 [27]. START08 was designed to study the chemical transport characteristics of the extratropical upper troposphere and lower stratosphere region. A total of 18 research flights covered a large region of North America (25–65°N in latitude and up to 14.3 km vertical range). Methane was measured *in situ* by the Unmanned Aircraft Systems Chromatograph for Atmospheric Trace Species. The 2-channel gas chromatograph employed a N2O-doped electron capture detector to measure methane at intervals of 140 s. The measurements were calibrated in-flight using whole air standards.

(5) The ARCTAS mission was conducted in April and June–July 2008 by the Global Tropospheric Chemistry Program and the Radiation Sciences Program of NASA. Its objective was to better understand the factors driving current changes in Arctic atmospheric composition and climate. Three research aircrafts (DC-8, P-3, B-200) were used and a total of 24 research flights had been made. The aircraft were based in Alaska in April (ARCTAS-A) and in western Canada in June–July (ARCTAS-B). The DACOM instrument used is an infrared tunable diode laser absorption spectrometer which makes measurements of CH4 (as well as CO and N_2O) at a 1 Hz sample rate. The CH4 accuracy is tied to NOAA/ESRL/GMD carbon cycle group standards and is nominally 1%, and the precision is 0.1% (1 sec, 1 sigma). CH4 observations during ARCTAS-A showed little variability and no indication of significant April emissions from Arctic ecosystems. The July observations in ARCTAS-B over the Hudson Bay Lowlands revealed higher wetland emissions of methane than previously recognized [28].

Table 1. 26 Sites of NOAA/ESRL/GMD aircraft measurements and the number of aircraft profiles used for validation. The profiles are used when there are valid AIRS retrieved profiles within 800 km in the same day in our gridded run data.

CODE	Location	Latitude, Longitude	Profiles used
AAO	Bondville, IL, United States	40.05, −88.37	202
BGI	Bradgate, IA, United States	42.82, −94.41	23
BNE	Beaver Crossing, NE, United States	40.80, −97.18	73
BRM	BERMS, SK, Canada	54.34, −104.99	9
CAR	Briggsdale, CO, United States	40.37, −104.30	124
CMA	Cape May, NJ, United States	38.83, −74.32	87
DND	Dahlen, ND, United States	48.14 , −97.99	76
ESP	Estevan Point, BC, Canada	49.58, −126.37	131
ETL	East Trout Lake, SK, Canada	54.35, −104.98	90
FWI	Fairchild, WI, United States	44.66, −90.96	24
HAA	Molokai Island, HI, United States	21.23, −158.95	45
HFM	Harvard Forest, MA, United States	42.54, −72.17	49
HIL	Homer, IL, United States	40.07, −87.91	85
LEF	Park Falls, WI, United States	45.93, −90.27	122
NHA	Worcester, MA, United States	42.95, −70.63	67
NWR	Niwot Ridge, CO, United States	40.05, −105.58	45
OIL	Oglesby, IL, United States	41.28, −88.94	35
PFA	Poker Flat, AL, United States	65.07, −147.29	72
RIA	Rowley, IA, United States	42.40, −91.84	26
RTA	Rarotonga, Cook Islands	−21.25, −159.83	42
SCA	Charleston, SC, United States	32.77, −79.55	83
SGP	Southern Great Plains, OK, United States	36.80, −97.50	128
TGC	Sinton, TX, United States	27.73, −96.86	82
THD	Trinidad Head, CA, United States	41.054, −124.151	70
VAA	Cartersville, GA, United States	32.91, −79.36	8
WBI	West Branch, IO, United States	41.725, −91.353	72

AIRS averaging kernels have been applied to the *in situ* aircraft data for validation [23]. Because of the limits of aircraft altitude, the *in situ* profiles provided by NOAA/ESRL/GMD are mostly below the

most sensitive region of AIRS and do not span the entire vertical range defined by the AIRS weighting functions. Extrapolation to the aircraft profiles is required to generate validation profiles. In this paper we used the monthly averaged CH_4 data from an Atmospheric General Circulation Model (AGCM)-based chemistry transport model (hereinafter ACTM) [29] to extrapolate from the top of the *in situ* aircraft profile to the top of atmosphere.

For the validation exercise using NOAA/ESRL/GMD aircraft data, we simply used AIRS gridded run data archived at NOAA/NESDIS/STAR, and the collocated AIRS retrieved profiles from AIRS ascending mode (1:30 pm local time) were selected if they are within 800 km of each site. For the validation exercise using campaign data, we computed AIRS retrievals at the standard product spatial resolution of 45 km, and the collocated AIRS retrieved profiles were selected if they are within 200 km of aircraft measurements. The mean of the collocated profiles were compared with *in situ* aircraft measurements (convolved using the averaging kernels).

3.2. Validation Results

Figure 3 shows the validation using data from eight sites of NOAA/ESRL/GMD aircraft measurements, and a combination of aircraft data from 26 sites (Table 1). The eight sites used as examples were selected from southmost (*i.e.*, RTA) to northmost (*i.e.*, PFA) among these 26 sites. Since the upmost level of these aircraft measurements is usually below 350 hPa, only the data at layer 359–460 hPa are compared in Figure 3. However, this layer is below the most sensitive layers of AIRS, which is at about 200–400 hPa in the tropics and mid-latitude regions, so the correlation between the AIRS retrievals and the aircraft measurements should be smaller than expected if using data in the most sensitive layers. The correlation coefficients are about 0.5–0.6 for sites near the tropics and mid-latitude regions, and decrease significantly in the high latitude regions, *i.e.*, 0.39 for site ETL (54.35°N) and 0.14 for site PFA (65.07°N). The RMSE also increases from ~0.5–0.7% in the tropics and mid-latitude regions to 0.94% for high latitude site ETL and 1.02% for site PFA. After merging all data in 26 sites, the correlation coefficient of AIRS retrieval with observation is 0.65 and RMSE is 0.73%. These results are obviously hampered by the non-ideal validation data used, in which the temporal difference between AIRS and *in situ* aircraft measurements is at least a couple of hours, and the spatial difference is as large as 800 km. Even so, these results indicate that space-borne observation by AIRS has a certain capability to map the variation of CH_4 in the mid-upper troposphere, but this capability deteriorates towards the polar region. One reason for the low correlation coefficient in the high northern latitude regions is associated with the large difference in spatial collocation of AIRS observations (within 800 km) with aircraft measurements as the air masses in such a big area with a radius of 800 km are more likely different in the polar regions than in the mid-latitude regions, and using campaign data from ARCTAS, the correlation is much better, as will be shown in Figure 4.

Compared to validation made in Xiong *et al.* [19] that used 671 profiles, more recent aircraft measurements from NOAA/ESRL/GMD since February, 2006 were used. The retrieval algorithm is almost the same, except for some minor changes in channels. Some minor patches/changes in the whole retrieval system have also been made, and the impact of these changes is insignificant on CH_4 results. One of the more significant changes in the retrieval was to accommodate the noise degradation in AMSU Channel 4, which impacts the cloud-clearing and retrievals of temperature, moisture and

surface emission, which, in turn, may impact the quality of all AIRS products. However, a rough estimate of AIRS CH_4 quality based on the validation error and correlation coefficient in different years from 2004 to 2009 does not show any trend in the retrieval bias and RMSE, so the quality of AIRS CH_4 product so far is relatively stable.

Figure 3. Scatter plot of AIRS *vs in situ* aircraft observations of CH_4 at layer 359–460 hPa for 8 sites separately and a mix of all profiles from 26 sites from August 2003 to December 31, 2009 (N = 1,813). The dashed line is the 1:1 line, and the Pearson correlation coefficient (R), bias and RMSE (in parenthesis) are given. X-axis is the *in situ* aircraft observations.

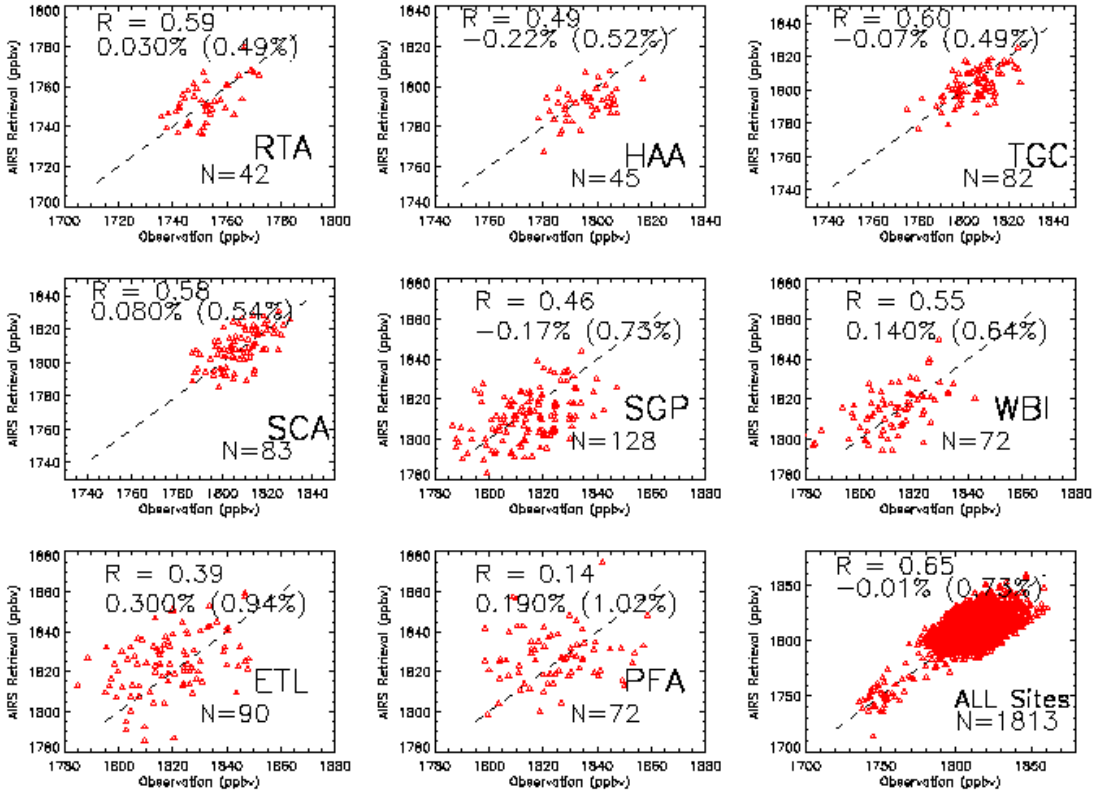

In Figure 4 data from several campaigns were used. Compared to aircraft measurements from NOAA/ESRL/GMD sites in Figure 3, these aircraft measurements mostly took samples to higher altitudes up to 200 hPa. So, in addition to the data at layer 359–460 hPa, data in a higher layer at 260–359 hPa is also compared. Except in the upper layer in INTEX-B, the correlation coefficients are mostly larger than in Figure 3. The most significant improvement is in the high northern latitude regions, as illustrated from ARCTAS data in the bottom two panels. However the RMSE in ARCTAS data is still larger than in middle-lower latitude regions.

Figure 4. Same as Figure 3 but for two layers at 260–359 hPa and 359–460 hPa, respectively and using aircraft observations from campaigns INTEX-A, INTEX-B, START08 and ARCTAS.

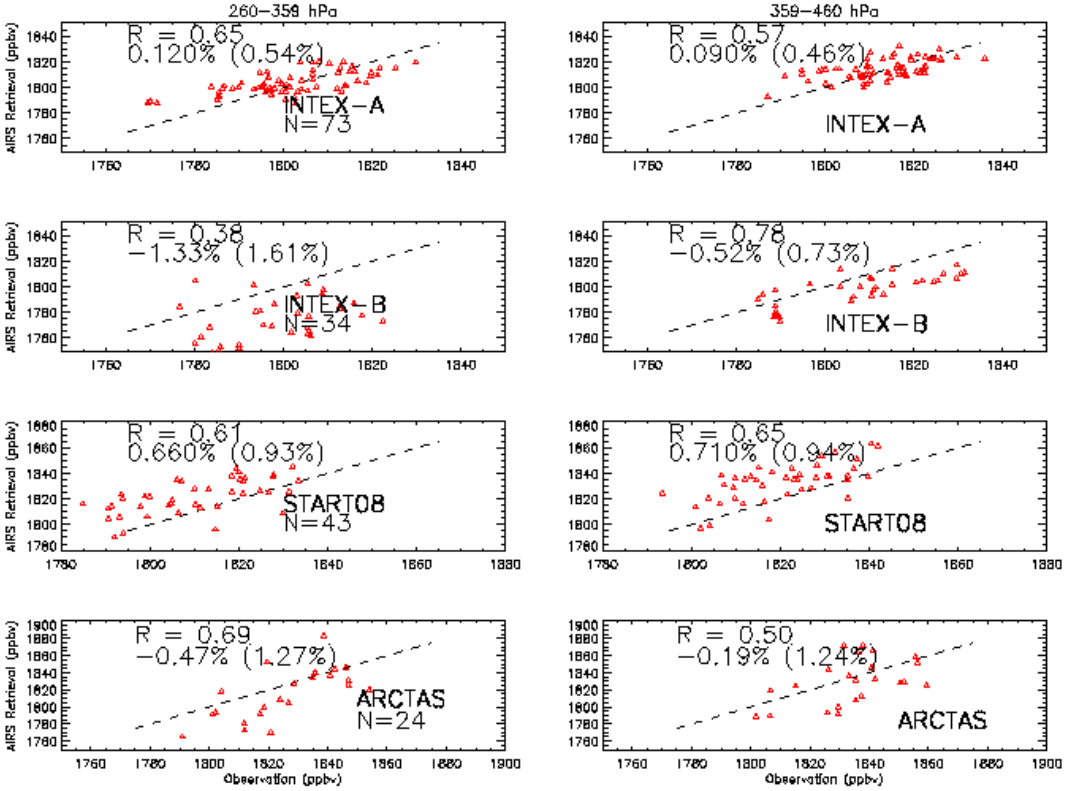

3.3. The Representative Layer in the AIRS Retrieved CH_4 Profile for Scientific Analysis in the HNH

CH_4 is well mixed in the troposphere; however, it has a large vertical gradient in the boundary layer and near tropopause. In the most CH_4 sensitive layer of AIRS in the mid-upper troposphere, variation of CH_4 mixing ratio is relatively small. Such a characteristic allows us to use the AIRS retrieved CH_4 mixing ratio in its most sensitive layer for analyzing the variation of MUT-CH_4, which is obviously better than using the AIRS retrieved CH_4 in a fixed pressure layer. As detailed by Xiong *et al.* [21], in the HNH the most sensitive layer of AIRS to CH_4 has a good correlation with the tropopause, thus a layer 50 to 250 hPa below tropopause, which is defined as the "Representative Layer" of AIRS, was chosen for scientific analysis. We noted that when the tropopause is very low, for example at 400 hPa in the polar region, the layer 50 to 250 hPa below tropopause will be at 450 to 650 hPa, which may be out of the most sensitive region of AIRS and the impact from surface emission could be significant (with a large vertical gradient of CH_4 mixing ratio near 650 hPa). So, in this paper we define the top level as $500*(Ptrop)^{-0.5}$ and lower level as $2{,}500*(Ptrop)^{-0.5}$, where Ptrop is the pressure of tropopause. In such definition the "Representative Layer" is thinner in the high latitude regions than that defined in Xiong *et al.* [21].

As an example, using the data from the site PFA in the high northern latitude region, Figure 5 shows that the AIRS retrieved CH_4 in its "Representative Layer" has a much better correlation with *in situ* aircraft measurements, R = 0.47, as compared to that in a fixed pressure layer (see the middle

column and bottom panel in Figure 3, R = 0.14). The average pressure bounds of this "Representative Layer" at site PFA are between 302 hPa to 423 hPa. One reason for this better correlation is obviously associated with the average of the collocated AIRS data in a large region, as in this method the CH_4 from the same airmass is more likely averaged and the airmasses impacted by stratospheric intrusion or local emission are likely excluded. Given the relatively larger variation of tropopause and the exchange of air between the lower stratosphere and upper troposphere, it is more difficult to find a fixed pressure layer to represent the mid-upper troposphere where AIRS has a good sensitivity in the high northern latitude regions, so it is more reasonable to analyze the variation of AIRS MUT-CH_4 using the data in the "Representative Layer" than in a fixed pressure layer in the HNH where the information content of AIRS is relatively low.

Figure 5. Scatter plot of AIRS *vs in situ* aircraft observations in the "Representative Layer" of AIRS (defined as a layer 500*(Ptrop)$^{-0.5}$ to 2,500*(Ptrop)$^{-0.5}$ below tropopause, Ptrop) using the data at PFA only. The dashed line is the 1:1 line, and the Pearson correlation coefficient (R), bias and RMSE (in parenthesis) are given. X-axis is the *in situ* aircraft observations. The correlation coefficient is better than that in a fixed pressure layer, as shown in the middle column and bottom panel of Figure 3.

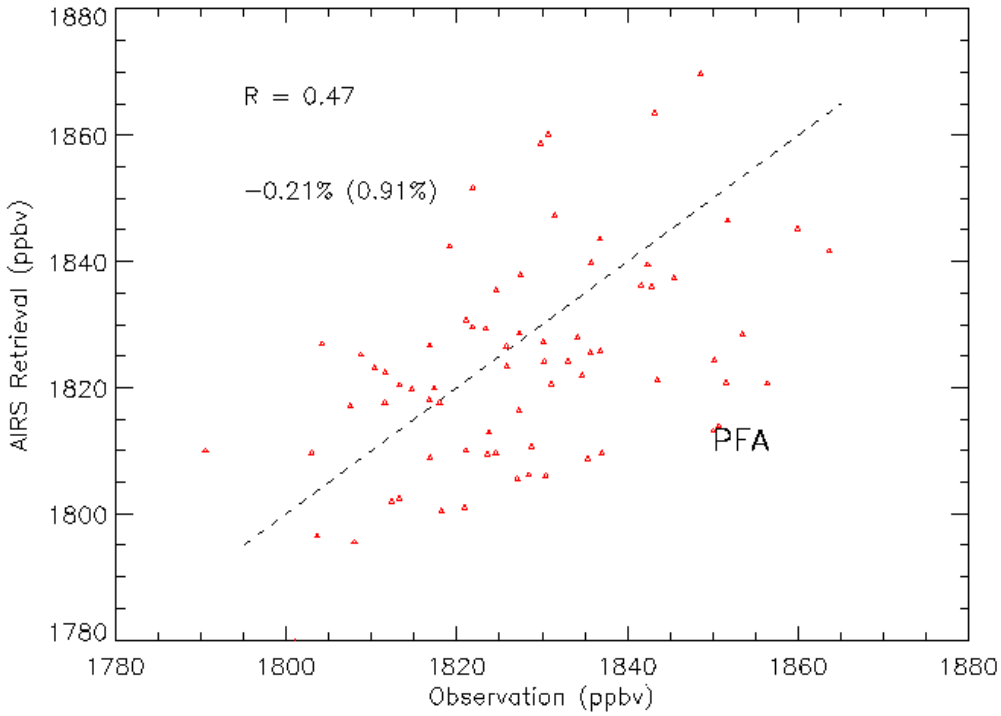

4. Multi-Year MUT-CH_4 Mixing Ratios from AIRS Observations, Seasonal Cycle and its Increase in 2008–2009

CH_4 mixing ratio in the atmosphere is almost stable after 2000, but a renewed increase was reported in 2007 and 2008 from the ground-based measurements in the MBL [7,8]. In this session we will analyze the trend of MUT-CH_4 from AIRS observations in the past 7 years from 2003 to 2009 and examine the response of mid-upper CH_4 tropospheric corresponding to the renewed increase of CH_4 in

the MBL in 2007–2008. A global view of its yearly change during 2007–2009 is shown in Figures 6 and 7. The trend of AIRS CH_4 and its comparison with ground-based measurements [30] for three focus regions in southern hemisphere, south Asia and the HNH will be discussed separately.

4.1. Global View of MUT-CH_4 and Its Increase during 2007–2009

Figure 6 shows the mean of MUT-CH_4 at layer 160–260 hPa and the annual increase in 2007, 2008 and 2009. The upper left panel is the difference of 2007 minus the mean during 2003–2006, and the upper right panel is the difference of 2009 minus 2008 and the lower left is the difference of 2008 minus 2007. The 2007 increase of CH_4 observed in the MBL is not evident in the mid-upper troposphere, however, the increase in 2008 is significant over the globe, and the largest increase of up to 15–20 ppbv occurs near the tropics. The 2008 increase in the HNH is up to 10 ppbv, but the increase in high southern hemisphere is small. From 2008 to 2009 MUT-CH_4 continued to increase in most regions, and the largest increase is in the high northern latitude regions, as shown in Figure 7 and Table 2. However, there is little increase near the tropics in 2009. Since the most sensitive layer of AIRS in the high latitude regions is towards to a lower altitude than in the mid-latitude regions and tropics, the annual change in the high latitude regions can be better shown from Figure 7. Table 2 lists the amount of increase of MUT-CH_4 in two layers and in three regions during 2007–2009. The locations of these three regions are shown in upper left panels in Figures 6 and 7.

Table 2. Annual change of MUT-CH_4 during 2007–2009 in layers 160–260 hPa and 260–359 hPa (in parenthesis) for three regions. The change of the CH_4 mixing ratios in 2007 is obtained by subtracting the mean from 2003 to 2006 (unit: ppbv).

	2007	2008	2009
Alaska-Canada	−0.32(1.06)	5.42(4.93)	5.89(5.11)
South Asia	−1.58 (0.93)	12.89(7.0)	−0.29 (0.09)
South Hemisphere	−1.63(−0.48)	1.92(3.06)	3.53(1.65)

Figure 6. Global distribution of MUT-CH_4 for layer at 160–260 hPa during 2003–2006 and its annual change during 2007–2009. The color bar in the lower left is for the annual change, and the color bar in the lower right is for the mean distribution.

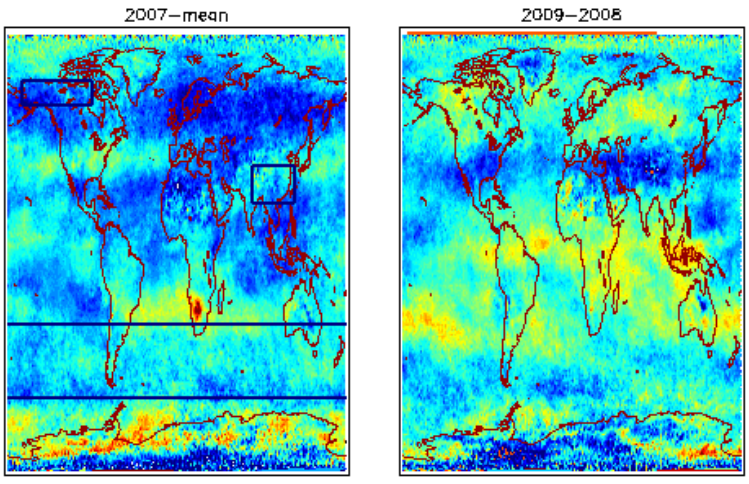

Figure 6. *Cont.*

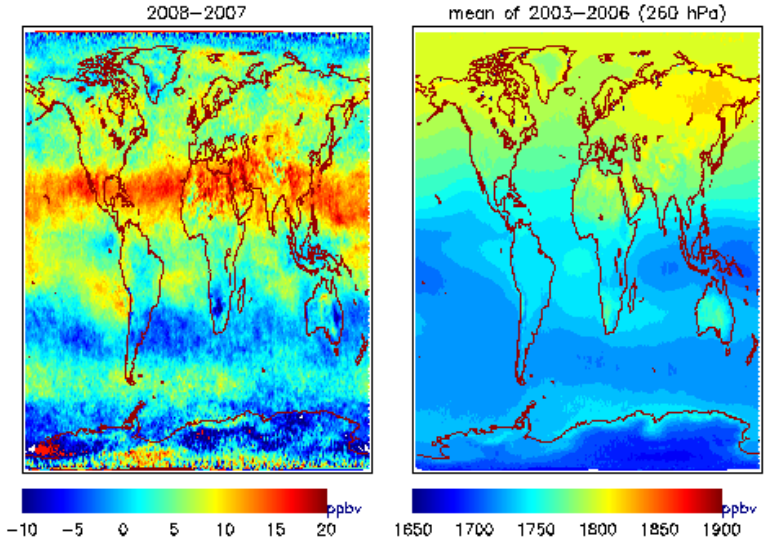

Figure 7. Same as Figure 6 but for layer at 359 hPa.

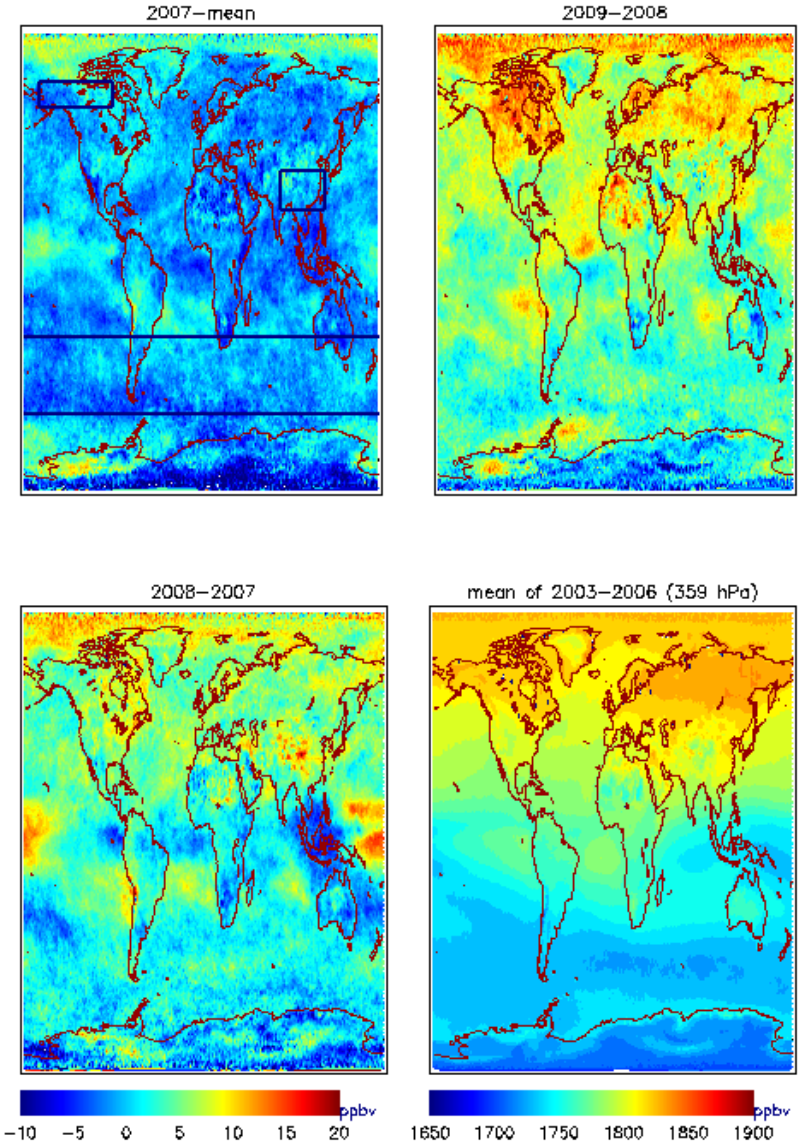

4.2. MUT-CH_4 in Southern Hemisphere

In the southern hemisphere, vertical variation of CH_4 is small or has little increase with altitude in the mid-lower troposphere due to the long-range transport from northern hemisphere [19]. As shown in the upper panel in Figure 8, it is reasonable that AIRS retrieved CH_4 at 258–358 hPa is close to CH_4 in the MBL measured at site Cape Grim, Tasmania, Australia (CGO, −40.6830°S 144.6900°E, 94 m). To derive the trend of MUT-CH_4, we need to remove its seasonal cycle first. The method used in this paper is to compute the monthly mean using data from 2003 to 2006, and subtract it to derive the CH_4 anomaly since 2007. The linear trend from 2006 to 2009 is obtained through linear-fitting to CH_4 anomaly with time. The trend of MUT-CH_4 from AIRS from 2006 to 2009 is 3.3 ± 0.4 (1σ) ppbv/yr, which is lower than CH_4 in the MBL, 6.3 ± 0.5 ppbv/yr, by 41%.

Figure 8. The upper panel is the seasonal variation of CH_4 for layer at 258–358 hPa (black) over the Southern Hemisphere and its comparison with CH_4 in the MBL at site CGO (red). The lower panel is the CH_4 anomaly (dots) deseaonalized using the monthly mean from 2003 to 2006, and the solid lines are the linear trend from 2006 to 2009.

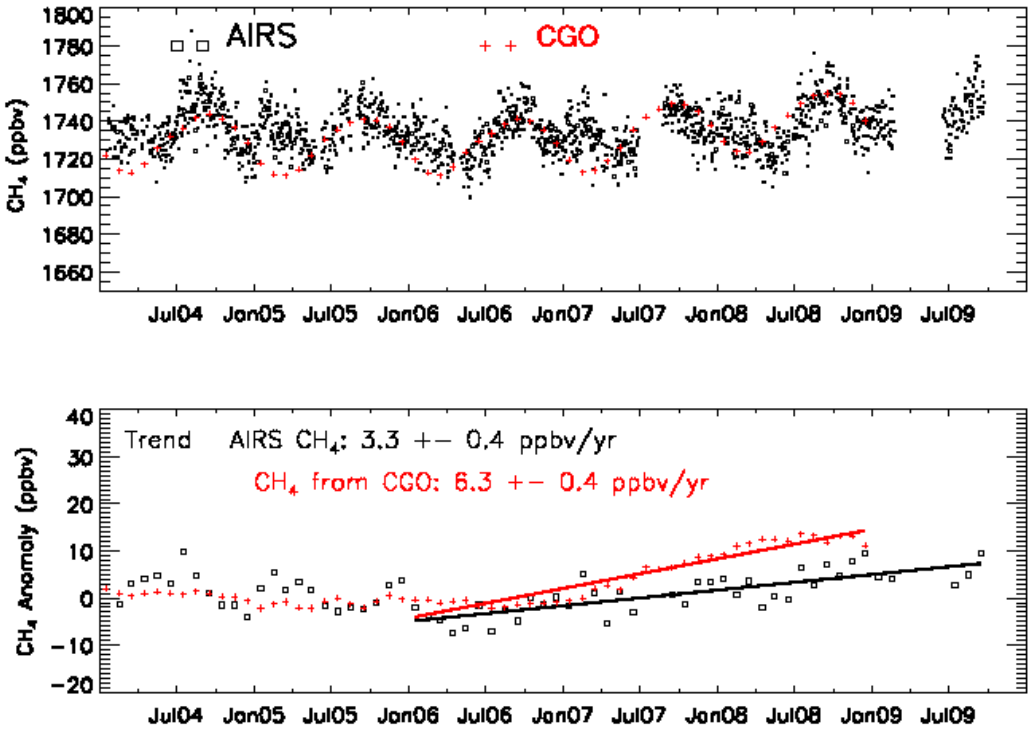

4.3. MUT-CH_4 in South Asia

It was found by Xiong *et al.* [31] that over the South Asia AIRS CH_4 has a strong, plume-like enhancement in the middle to upper troposphere during July, August and September, with the maximum occurring in early September. The seasonal variation of AIRS CH_4 is consistent with model simulation, as shown in Figure 9 (upper panel). Here ACTM refers to an Atmospheric General Circulation Model (AGCM)-based chemistry transport model [22]. The *in situ* measurements from the Civil Aircraft for the Regular Investigation of the atmosphere Based on an Instrument Container

(CARIBIC), a project to study and monitor important chemical and physical processes in the Earth's atmosphere, provide evidence for the enhancement of CH_4 during the summer [32]. The highest MUT-CH_4 in late summer is close to the ground-based measurements in Mt. Waliguan, China (WLG, 36.2879°N 100.8964°E, 3,810 m) while the annual average of MUT-CH_4 is about 70 ppbv lower than ground-based measurements. The linear trend for MUT-CH_4 from 2006 to 2009, 6.2 ± 1.3 ppbv/yr, is very close to the trend of CH_4 in the WLG from 2006 to 2008. However, different from CH_4 in the MBL that starts to increase in 2007, significant increase of MUT-CH_4 is evident in 2008. Also, AIRS MUT-CH_4 shows a decrease in 2005, which is not obvious from the ground-based measurements.

Figure 9. The upper panel is the seasonal variation of the MUT-CH_4 at layer 160–259 hPa (black line is the running mean over a biweekly window) and its comparison with the model simulation by ACTM (Green line) and ground-based measurements of CH_4 mixing ration at site WLG(red crosses). The lower panel shows the anomaly of MUT-CH_4 and CH_4 at WLG and the linear trend for both of them (solid red line and black line are almost overlapped).

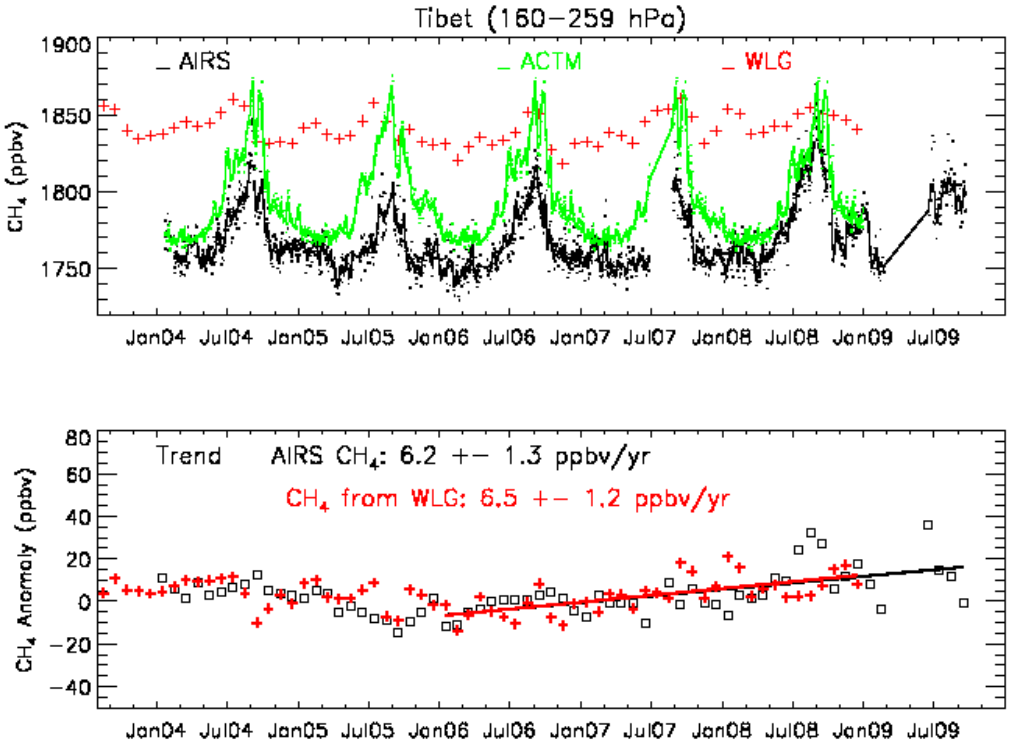

4.4. MUT-CH_4 in the HNH

The mixing ratio of MUT-CH_4 from AIRS is about 60 ppbv lower than CH_4 in the MBL measured at site Barrow, Alaska, USA (BRW). The low value of MUT-CH_4 in May agrees with the decrease of CH_4 in the MBL. However, MUT-CH_4 starts to increase in June–July due to the enhanced vertical convection, and possibly a combination from the enhanced emissions from wetlands or permafrost regions. On the contrary, due to the photochemical reaction, the CH_4 in the MBL reaches the minimum in the summer. This summer minimum for CH_4 in the MBL is not evident from the AIRS observed MUT-CH_4, even though sometimes the low mixing ratios were observed from NOAA/ESRL/GMD

aircraft measurements, but relatively high mixing ratios were also observed in some other times. The trend of MUT-CH_4 from AIRS from 2006 to 2009 in the high northern latitude region is 3.9 ± 1.0 ppbv/yr, which is close to that in the Southern Hemisphere, but lower than the CH_4 in the MBL at Barrow, Alaska (BRW). Both the AIRS retrievals and ground measurements are more scattered than in Figure 8, which is associated with the larger emission sources in the HNH. As in the South Asia, AIRS MUT-CH_4 shows a decrease in 2005, and in agreement with AIRS, the ground-based measurements also show similar decrease in this period.

Figure 10. Same as Figure 8 but using ground-based measurements at site BRW, and MUT-CH_4 is derived from the AIRS retrieved CH_4 in the "Representative Layer" of AIRS.

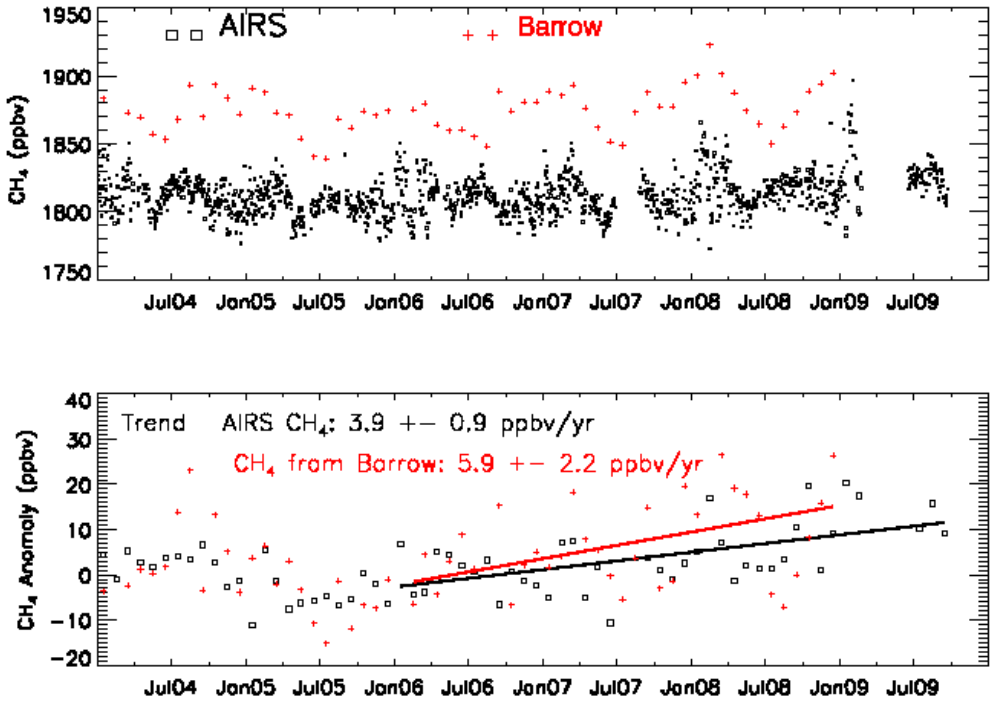

4.5. Seasonal Cycle of MUT-CH_4

Using the data in Figures 8–10, we computed the monthly average of MUT-CH_4 and CH_4 during 2004 to 2009 to get their seasonal cycles. As described by Xiong *et al.* [22], the seasonal cycle of MUT-CH_4 in the HNH is nearly opposite to CH_4 in the MBL, and particularly MUT-CH_4 has a summer high while CH_4 in the MBL reaches the minimum in summer. This difference of seasonal cycle is evident from the top panel of Figure 11. The CH_4 mixing ratios in the MBL are about 70–80 ppbv higher than in the mid-upper troposphere during the winter-spring seasons, but in June–July this difference is reduced by about 50%. Both of them show a decrease from March to May, and MUT-CH_4 reaches its seasonal minimum in May, but the minimum of CH_4 in the MBL occurs in July, which is driven by the photochemical loss of CH_4. The summer increase of MUT-CH_4 is mainly driven by the enhanced upward convection in this period. Obviously, the increase of CH_4 emission from the high northern ground, especially in the early summer, will impact the CH_4 in the mid-upper troposphere, which, in turn, will join in the global circulation and impact the climate.

In the southern hemisphere (data shown in the middle panel of Figure 11 is 30°S–60°S), the difference of the seasonal cycle of MUT-CH_4 with CH_4 in the MBL lies in the January–March. This is the summer time in the southern hemisphere, and as driven by the photochemical loss, CH_4 in the MBL reaches the minimum in February. However, the photochemical loss of MUT-CH_4 is not as strong as the loss of CH_4 in the MBL, because of the dependence of photochemical reaction with temperature. Under the impact of mixing of CH_4 in the mid-upper troposphere with CH_4 in the MBL, which is lower than MUT-CH_4, the MUT-CH_4 keeps decreasing after February to May. Both the MUT-CH_4 and CH_4 in the MBL increase in June, July and August.

Figure 11. Seasonal cycles of MUT-CH_4 in Alaska-Canada, South Hemisphere and South Asia and its comparison with ground-based measurements of CH_4 at sites CGO, Barrow and WLG. Due to the difference of CH_4 mixing ratio between the surface and mid-upper troposphere, 60 ppbv is subtracted from the ground-based measurements at Barrow, and 70 ppbv is subtracted from ground-based measurements at WLG.

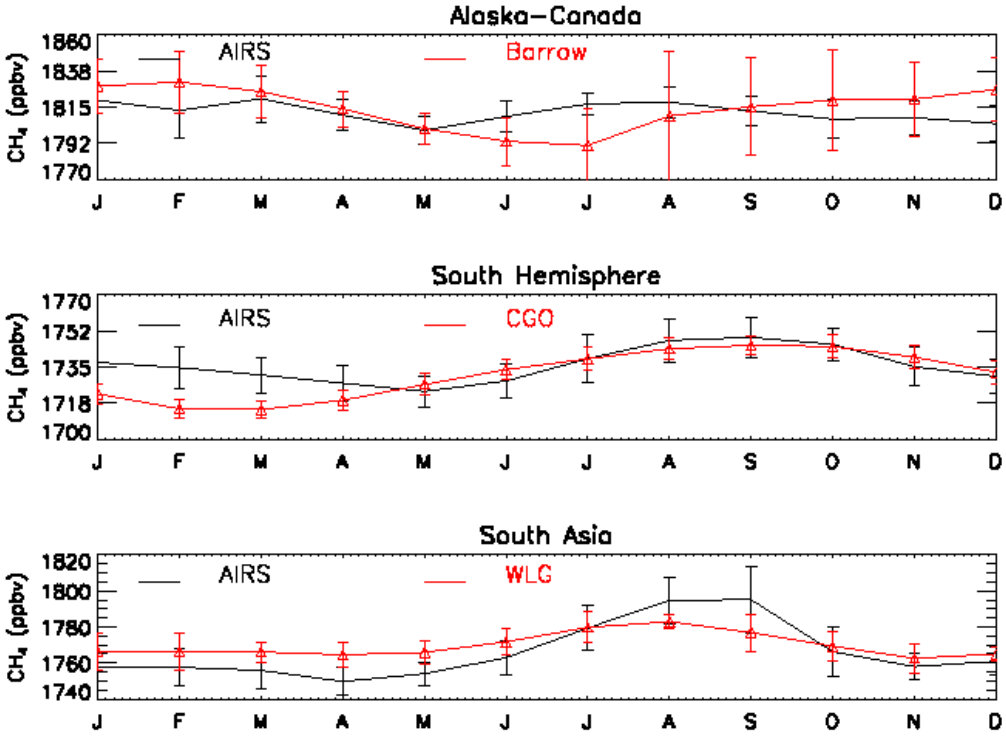

In the South Asia, there is a good agreement in the summer increase of MUT-CH_4 and CH_4 in the MBL. However, the amplitude of seasonal change for CH_4 in the MBL is smaller than MUT-CH_4. The maximum of CH_4 from ground-based measurements in Mt. Waliguan occurs in August, and the maximum of MUT-CH_4 occurs in early September [21] due to the increased emission from rice paddies in China, upward transport via deep convection, and the confinement by the anticyclone. With the withdrawing of the Asian summer monsoon, the anticyclone dissipates quickly, leading to the dispersion of CH_4 in the mid-upper troposphere.

5. Summary and Conclusions

As a thermal infrared sounder, AIRS on EOS/Aqua platform has provided a unique measurement of mid-upper tropospheric CH_4 (MUT-CH_4) since September 2002. From the analysis of AIRS sensitivity, it is clear that AIRS is capable of detecting a less than 2% change of atmospheric CH_4 total column in the tropics and mid-latitude regions, but its capability deteriorates to about 2% or more in the polar region. Validation with *in situ* aircraft measurements demonstrated that the retrieval RMSEs are mostly less than 1.5%; however, this validation is limited due to the poor collocation of AIRS data with aircraft measurements, including the altitude limit, time discrepancy (at least a few hours) and spatial coverage. The number of aircraft measurements in the southern hemisphere and high northern latitude regions is limited for validation. Overall, the AIRS CH_4 product is stable during the period from 2003 to 2009, so we used this product to examine the trend of mid-upper tropospheric CH_4, particularly to investigate the response of MUT-CH_4 to the recent increase of atmospheric CH_4 near the surface.

One challenge in the use of AIRS observation of CH_4 is due to the limited information content from thermal infrared sounder, and the degree of freedom (DOF) of the retrieval is about 1.0. In the high northern latitude regions, it was found that the DOF is correlated with the tropopause height, *i.e.*, when the tropopause height is higher in summer season, the DOF is larger and AIRS has a better sensitivity to detect the variation of atmospheric CH_4. Due to the change of AIRS sensitivity with altitude and season, the AIRS retrieved CH_4 in the "Representative Layer" was used for analysis in the HNH. The advantages of using "Representative Layer" CH_4 for analysis are: (1) it represents the retrievals near the most sensitive layer; (2) it avoids the interference of stratospheric intrusion and/or minimize the impact from surface emission. The improvement in the correlation coefficient between AIRS CH_4 and *in situ* measurements in the "Representative Layer" suggests that this use of CH_4 in "Representative Layer" is valuable. Due to the difficulty in retrieving CH_4 in the high northern latitude regions, more work is still required to improve the retrievals, validation and usage of the retrievals for scientific analysis.

Analysis of deseasonalized time-series of AIRS CH_4 in both a fixed pressure layer and the "Representative Layer" in the HNH from 2003 to 2009 indicates that the MUT-CH_4 increases about 3–6 ppbv/yr from 2006 to 2009, which is less than CH_4 observed in the MBL. The most significant increase of MUT-CH_4 is about 13 ppbv near tropics and south Asia in 2008, and it continues to increase in 2009 but with a smaller rate. In the HNH, the increase in 2009 is about 5–6 ppbv. Compared to CH_4 in the lower troposphere that has the most significant increase in 2007, the increase of MUT-CH_4 is delayed about 1 year. If the major driver of recent CH_4 increase is the increased surface emission, it will be easy for us to understand the delay of the MUT-CH_4 increase and its lower increase rate than the CH_4 observed in the MBL, as the mixing of the surface emission needs some time and the mixing in the whole atmosphere leads to its dilution in the whole atmosphere.

The seasonal cycles of MUT-CH_4 are different from CH_4 in the MBL, which suggests that in the mid- upper troposphere, the impact of transport is of equivalent importance as the surface emission and the photochemical loss in controlling the seasonal cycle. Unlike the CH_4 in the MBL that reaches the minima in both the northern latitude summer and the southern latitude summer, the MUT-CH_4 has a seasonal high. This summer increase of MUT-CH_4 in the HNH suggests that the enhanced summer

convection may provide a pathway for the CH_4 emitted from the high northern latitude regions, thus the release of CH_4 from northern wetlands, lakes and thawing permafrost may play a more important role for climate change than expected, and calls for more study.

Acknowledgements

This research was supported by funding from NOAA Office of Application & Research. The views, opinions, and findings contained in this paper are those of the authors and should not be construed as an official National Oceanic and Atmospheric Administration or U.S. Government position, policy, or decision. The data of INTEX-A and B used in this publication was obtained from Aura Validation Data Center (AVDC) (http://avdc.gsfc.nasa.gov/index.php) and the aircraft measurements of INTEX-NA were carried out by Donald R. Blake of Department of Chemistry, University of California, Irvine; and airborne CH_4 data from INTEX-B and ARCTAS were provided by Glen Sachse and Glenn Diskin of NASA Langley. ARCTAS data were downloaded from (ftp://ftp-air.larc.nasa.gov/pub/ARCTAS/). The CH_4 data of START08 aircraft measurements were carried out by Dale Hurst and Jim Elkins of NOAA/ESRL/GMD. We appreciate Colm Sweeney at NOAA/ESRL/GMD for providing the aircraft measurements data.

References

1. Solomon, S.; Qin, D.; Manning, M.; Chen, Z.; Marquis, M.; Averyt, K.B.; Tignor, M.; Miller, H.L. *Climate Change 2007: The Physical Science Basis: Contribution of Working Group I to the Fourth Assessment Report of the Intergovernmental Panel on Climate Change*; Cambridge University Press: Cambridge, UK and New York, NY, USA, 2007; p. 996.
2. Rasmussen, R.A.; Khalil, M.A.K. Atmospheric methane in recent and ancient atmospheres: Concentrations, trends, and interhemispheric gradient. *J. Geophys. Res.* **1984**, *89*, 11599-11605.
3. Nakazawa, T.; Machida, T.; Tanaka, M.; Fujii, Y.; Aoki, S.; Watanabe, O. Differences of the atmospheric CH_4 concentration between the Arctic and Antarctic regions in pre-industrial/pre-agricultural era. *Geophys. Res. Lett.* **1993**, *20*, 943-946.
4. Dlugokencky, E.J.; Steele, L.P.; Lang, P.M.; Masarie, K.A. The growth rate and distribution of atmospheric methane. *J. Geophys. Res.* **1994**, *99*, 17021-17044.
5. Dlugokencky, E.J.; Houweling, S.; Bruhwiler, L.; Masarie, K.A.; Lang, P.M.; Miller, J.B.; Tans, P.P. Atmospheric methane levels off: Temporary pause or a new steady-state? *Geophys. Res. Lett.* **2003**, *30*, doi: 10.1029/2003GL018126.
6. Simpson, I.J.; Chen, T.-Y.; Blake, D.R.; Rowland, F.S. Implications of the recent fluctuations in the growth rate of tropospheric methane. *Geophys. Res. Lett.* **2002**, *29*, doi:10.1029/2001GL014521.
7. Rigby, M.; Prinn, R.G.; Fraser, P.J.; Simmonds, P.G.; Langenfelds, R.L.; Huang, J.; Cunnold, D.M.; Steele, L.P.; Krummel, P.B.; Weiss, R.F.; O'Doherty, S.; Salameh, P.K.; Wang, H.J.; Harth, C.M.; Mühle, J.; Porter, L.W. Renewed growth of atmospheric methane. *Geophys. Res. Lett.* **2008**, *35*, doi: 10.1029/2008GL036037.

8. Dlugokencky, E.J.; Bruhwiler, L.; White, J.W.C.; Emmons, L.K.; Novelli, P.C.; Montzka, S.A.; Masarie, K.A.; Lang, P.M.; Crotwell, A.M.; Miller, J.B.; Gatti, L.V. Observational constraints on recent increases in the atmospheric CH_4 burden. *Geophys. Res. Lett.* **2009**, *36*, doi:10.1029/2009GL039780.
9. Zhuang, Q.; Melack, J.M.; Zimov, S.; Walter, K.M.; Butenhoff, C.L.; Khalil, M.A.K. Global methane emissions from wetlands, rice paddies, and lakes. *Eos Trans. AGU* **2009**, *90*, doi:10.1029/2009EO050001.
10. Walter, K.M.; Zimov, S.A.; Chanton, J.P.; Verbyla, D.; Chapin, F.S. Methane bubbling from Siberian thaw lakes as a positive feedback to climate warming. *Nature* **2006**, *443*, 71-75.
11. Shakhova, N.; Semiletov, I.; Salyuk, A.; Yusupov, V.; Kosmach, D.; Gustafsson, Ö. Extensive methane venting to the atmosphere from sediments of the East Siberian arctic shelf. *Science* **2010**, *327*, 1246-1250.
12. Frankenberg, C.; Bergamaschi, P.; Butz, A.; Houweling, S.; Meirink, J.F.; Notholt, J.; Petersen, A.K.; Schrijver, H.; Warneke, T.; Aben, I. Tropical methane emissions: A revised view from SCIAMACHY onboard ENVISAT. *Geophys. Res. Lett.* **2008**, *35*, doi:10.1029/2008GL034300.
13. Yokota, T.; Aoki, T.; Eguchi, N.; Ota, Y.; Yoshida, Y.; Oshchepkov, S.; Bril, A.; Desbiens, R.; Morino, I. Data retrieval algorithms of the SWIR bands of the TANSO-FTS sensor aboard GOSAT. *J. Remote Sens. Soc. Jpn* **2008**, *28*, 133-142.
14. Payne, V.H.; Clough, S.A.; Shephard, M.W.; Nassar, R.; Logan, J.A. Information-centered representation of retrievals with limited degrees of freedom for signal: Application to methane from the Tropospheric Emission Spectrometer. *J. Geophys. Res.* **2009**, *114*, doi:10.1029/2008JD010155.
15. Aumann, H.H.; Chahine, M.T.; Gautier, C.; Goldberg, M.D.; Kalnay, E.; McMillin, L.M.; Revercomb, H.; Rosenkranz, P.W.; Smith, W.L.; Staelin, D.H.; Strow, L.L.; Susskind, J. AIRS/AMSU/HSB on the aqua mission: Design, science objectives, data products, and processing systems. *IEEE Trans. Geosci. Remote Sens.* **2003**, *41*, 253-264.
16. Crevoisier, C.; Nobileau, D.; Fiore, A.M.; Armante, R.; Chédin, A.; Scott, N.A. Tropospheric methane in the tropics—First year from IASI hyperspectral infrared observations. *Atmos. Chem. Phys.* **2009**, *9*, 6337-6350.
17. Razavi, A.; Clerbaux, C.; Wespes, C.; Clarisse, L.; Hurtmans, D.; Payan, S.; Camy-Peyret, C.; Coheur, P.F.,Characterization of methane retrievals from the IASI space-borne sounder. *Atmos. Chem. Phys.* **2009**, *9*, 7889-7899.
18. Aumann, H.H.; Pagano, T.S. Using AIRS and IASI data to evaluate absolute radiometric accuracy and stability for climate applications. *Proc. SPIE* **2008**, *7085*, doi: 10.1117/12.795225.
19. Xiong, X.; Barnet, C.; Maddy, E.; Sweeney, C.; Liu, X.; Zhou, L.; Goldberg, M. Characterization and validation of methane products from the Atmospheric Infrared Sounder (AIRS). *J. Geophys. Res.* **2008**, *113*, doi: 10.1029/2007JG000500.
20. Strow, L.L.; Hannon, S.E.; De Souza-Machado, S.; Motteler, H.E.; Tobin, D. An overview of the AIRS radiative transfer model. *IEEE Trans. Geosci. Remote Sens.* **2003**, *41*, 303-313.
21. Xiong, X.; Barnet, C.; Wei, J.; Maddy, E. Information-based mid-upper tropospheric methane derived from Atmospheric Infrared Sounder (AIRS) and its validation. *Atmos. Chem. Phys. Discuss.* **2009**, *9*, 16331-16360.

22. Xiong, X.; Barnet, C.; Zhuang, Q.; Machida, T.; Sweeney, C.; Patra, P.K. Mid-upper tropospheric methane in the high northern hemisphere: Space-borne observations by AIRS, aircraft measurements and model simulations. *J. Geophys. Res*. **2010**, *115*, D19309.
23. Maddy, E.S.; Barnet, C.D. Vertical resolution estimates in Version 5 of AIRS operational retrievals. *IEEE Trans. Geosci. Remote Sens.* **2008**, *46*, 2375-2384.
24. Singh, H.B.; Brune, W.H.; Crawford, J.H.; Jacob, D.J.; Russell, P.B. Overview of the summer 2004 Intercontinental Chemical Transport Experiment-North America (INTEX-A). *J. Geophys. Res.* **2006**, *111*, doi:10.1029/2006JD007905.
25. Simpson, I.J.; Rowland, F.S.; Meinardi, S.; Blake, D.R. Influence of biomass burning during recent fluctuations in the slow growth of global tropospheric methane. *Geophys. Res. Lett.* **2006**, *33*, L22808.
26. Singh, H.B.; Brune, W.H.; Crawford, J.H.; Flocke, F.; Jacob, D.J. Chemistry and transport of pollution over the Gulf of Mexico and the Pacific: Spring 2006 INTEX-B campaign overview and first results. *Atmos. Chem. Phys.* **2009**, *9*, 2301-2318.
27. Pan, L.L.; Bowman, K.P. ; Atlas, E.L. ; Wofsy, S.C. ; Zhang, F.; Bresch, J.F.; Ridley, B.A.; Pittman, J.V.; Homeyer, C.R. ; Romashkin, P.; Cooper, W.A. The Stratosphere-Troposphere analyses of Regional Transport 2008 (START08) Experiment. *Bull. Amer. Meteor. Soc.* **2010**, *91*, 327-342.
28. Jacob, D.J.; Crawford, J.H.; Maring, H.; Clarke, A.D.; Dibb, J.E.; Ferrare, R.A.; Hostetler, C.A.; Russell, P.B.; Singh, H.B.; Thompson, A.M.; Shaw, G.E.; McCauley, E.; Pederson, J.R.; Fisher, J.A. The ARCTAS aircraft mission: design and execution. *Atmos. Chem. Phys. Discuss.* **2009**, *9*, 17073-17123.
29. Patra, P.K.; Takigawa, M.; Ishijima, K.; Choi, B.-C.; Cunnold, D.; Dlugokencky, E.J.; Fraser, P.; Gomez-Pelaez, A.J.; Goo, T.-Y.; Kim, J.-S.; Krummel, P.; Langenfelds, R.; Meinhardt, F.; Mukai, H.; O'Doherty, S.; Prinn, R.G. ; Simmonds, P.; Steele, P.; Tohjima, Y.; Tsuboi, K.; Uhse, K.; Weiss, R.; Worthy, D.; Nakazawa, T. Growth rate, seasonal, synoptic, diurnal variations and budget of methane in lower atmosphere. *J. Meteorol. Soc. Jpn.* **2009**, *87*, 635-663.
30. *GLOBALVIEW-CH4: Cooperative Atmospheric Data Integration Project—Methane*; [CD-ROM], NOAA ESRL: Boulder, CO, USA, 2009.
31. Xiong, X.; Houweling, S.; Wei, J.; Maddy, E.; Sun, F.; Barnet, C. Methane plume over south Asia during the monsoon season: Satellite observation and model simulation. *Atmos. Chem. Phys.* **2009**, *9*, 783-794.
32. Schuck, T.J.; Brenninkmeijer, C.A.M.; Baker, A.K.; Slemr, F.; von Velthoven, P.F.J.; Zahn, A. Greenhouse gas relationships in the Indian summer monsoon plume measured by the CARIBIC passenger aircraft. *Atmos. Chem. Phys.* **2010**, *10*, 3965-3984.

© 2010 by the authors; licensee MDPI, Basel, Switzerland. This article is an open access article distributed under the terms and conditions of the Creative Commons Attribution license (http://creativecommons.org/licenses/by/3.0/).